Supporting Information for

Tunable Pt-NiO interaction-induced efficient electrocatalytic water oxidation and methanol oxidation

Fenglin Wang,[a, b] Zhicheng Zheng,[b] Dan Wu,[b] Hao Wan,[a] Gen Chen,[b] Ning Zhang,[b] Xiaohe Liu,*[a, b] Renzhi Ma*[c]*

[a] Zhongyuan Critical Metals Laboratory, Zhengzhou University, Zhengzhou 450001, P. R. China. E-mail: wanhao@zzu.edu.cn (H. W.); liuxh@csu.edu.cn (X. L.)
[b] School of Materials Science and Engineering, Key Laboratory of Electronic Packaging and Advanced Functional Materials of Hunan Province, Central South University, Changsha, Hunan 410083, P. R. China.
[c] Research Center for Materials Nanoarchitectonics (MANA), National Institute for Materials Science (NIMS), Tsukuba, Ibaraki 305-0044, Japan. E-mail: MA.Renzhi@nims.go.jp (R. M.)

Experimental information

All chemicals of nickel nitrate hexahydrate ($Ni(NO_3)_2 \cdot 6H_2O$, Sinopharm Group Co. Ltd, China), hexamethylenetetramine (HMT, Alfa Aesar, China), sodium dodecyl sulfate (SDS, $C_{12}H_{25}O_4NaS$, Wako Pure Chemical Industries, Ltd.) were of analytical grade and directly used without additional purification.

Synthesis of α-Ni(OH)$_2$-DS.

First, 4 mmol of $Ni(NO_3)_2 \cdot 6H_2O$, 10 mmol of SDS and 24 mmol of HMT were dissolved in a three-neck flask containing 100 mL of Milli-Q deoxygenated water under a nitrogen flow in a reflux condenser. Then the synthetic process was carried out at a refluxing temperature of 120 °C under continuous stirring for 24 h. Cooling down naturally, the green product was filtered, washed with water and ethanol for several

times, and then dried in air at room temperature. Finally, *α-Ni(OH)$_2$-DS* product was obtained.

Synthesis of porous NiO-Pt$_{SA}$, NiO-Pt$_{cluster}$ and NiO-Pt$_{particle}$ samples.

The as-obtained *α-Ni(OH)$_2$-DS* product was calcined in air to prepare porous NiO with abundant defect sites at 700 ℃ for 3 h. NiO-Pt$_{SA}$ was prepared by mixing NiO and aqueous H_2PtCl_6 solution with a molar ratio of 10 : 1 and stirring for 48h in dark, which was beneficial to immobilize the Pt single atoms on NiO substrate via adsorption-impregnation strategy. The synthetic process of NiO-Pt$_{cluster}$ and NiO-Pt$_{particle}$ was the same as NiO-Pt$_{SA}$, except that they were stirred with xenon light for another 1 h and 3 h respectively after stirring 48 h under shading.

Materials Characterization.

Crystal compositions were investigated by X-ray diffraction (XRD, Rigaku D/max 2500) operated at 40 kV/15 mA with Cu Kα radiation (λ =1.54178 Å). Micro-/nano-structural and elemental information was detected by a scanning electron microscope (SEM, Sirion 200) and aberration-corrected high-angle annular darkled-scanning transmission electron microscopy (AC-HAADF-STEM, Tecnai G2 F20). X-ray photoelectron spectroscopy (XPS) signals were collected by Thermo Fisher ESCALAB 250Xi spectrophotometer. Details of the Pt phase were characterized with X-ray absorption fine structure (XAFS) spectra. Pt L_3-edge analyses were performed with the BL11B beamlines at the Shanghai Synchrotron Radiation Facility (SSRF, Shanghai, China). All XAS data were analyzed using Athena to subtract background signal to obtain normalized XANES and EXAFS information.

DFT calculations

Density functional theory (DFT) calculations were performed by the Vienna Ab initio Simulation Package (VASP) with the projector augmented wave (PAW) method. Generalized gradient approximation (GGA) of Perdew-Burke-Ernzerhof (PBE) functional was used for the exchange-functional. A vacuum spacing of 20 Å in a direction perpendicular to the plane of the catalyst was used to avoid interaction between units. The Brillouin zone integration was performed using 3 × 3 × 1 Monkhorst-Pack k-point sampling for a structure. The cut-off energy of the plane-wave

basis was set as 400 eV. The self-consistent calculations applied a convergence energy threshold of 10^{-4} eV. The vibrational frequencies were calculated to consider the zero-point energies, enthalpy, and entropy and ultimately calculate the free energies at room temperature (298.15 K).

Electrochemical measurements

Electrochemical OER measurements were conducted at a CHI 760E electrochemical workstation coupled with a typical three-electrode system using 1.0 M KOH electrolyte, graphite rod as the counter electrode and Hg/HgO electrode as the reference electrode. To prepare the working electrode, 2.5 mg of catalyst was dispersed in the mixture of water, ethanol and Nafion soluiton (5 wt%) with a volume ratio of 10 : 10: 1. Then the catalyst ink was dripped on the carbon paper, and then dried at 60 ℃ to achieve the mass loading of 0.5 mg cm^{-2}. All the potentials were calibrated with respect to the reversible hydrogen electrode (RHE) scale according to the equation: $E_{RHE} = E_{Hg/HgO} + 0.059 \times pH + 0.098$ V. Linear sweep voltammetry (LSV) was carried out at a scan rate of 5 mV s^{-1} with 95% iR compensation correction. The electrochemical impedance spectra (EIS) were recorded in the frequency range from 100 000 to 0.1 Hz with an amplitude of 5 mV. While for MOR test, a mixed 1.0 M KOH + 1.0 M CH_3OH aqueous electrolyte was adopted. The MOR activity was evaluated by CV scan with a scan rate of 50 mV s^{-1}. Chronoamperometric measurements were carried out at the constant potential of 0.70 V vs RHE.

TOF (s^{-1}) and production rate of O_2 (cm^{-2} s^{-1}) were calculated through the following equations:

$$\text{TOF} = (J \times A) \div (4 \times F \times n)$$

$$\text{Production rate of } O_2 = (J \times N_A) \div (z \times F)$$

where J (A cm^{-2}) was the current density, A (cm^{-2}) represented the loading area, F stood for the Faraday constant (96485 C mol^{-1}), n (mol) was the amount of substance, N_A corresponded to the Avogadro number (6.02 × 1023 mol^{-1}) and z (4) was the number of electrons for OER.

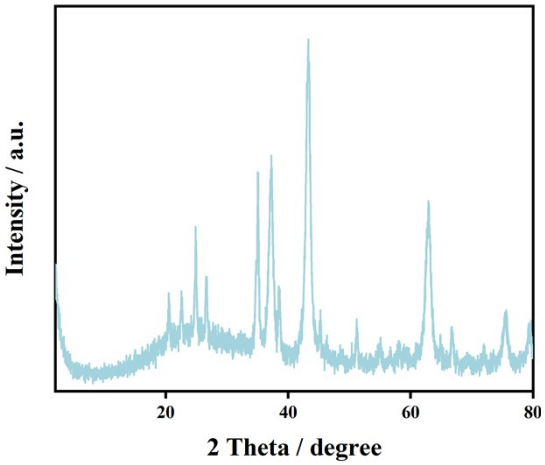

Figure S1. XRD pattern of porous NiO by calcining α-$Ni(OH)_2$ at 600˚C.

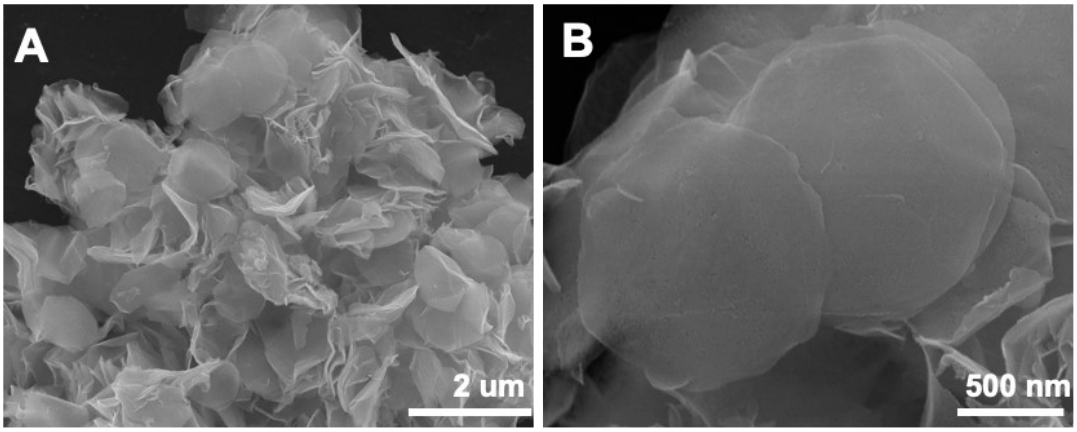

Figure S2. SEM images of the calcined product at 600˚C with different magnifications.

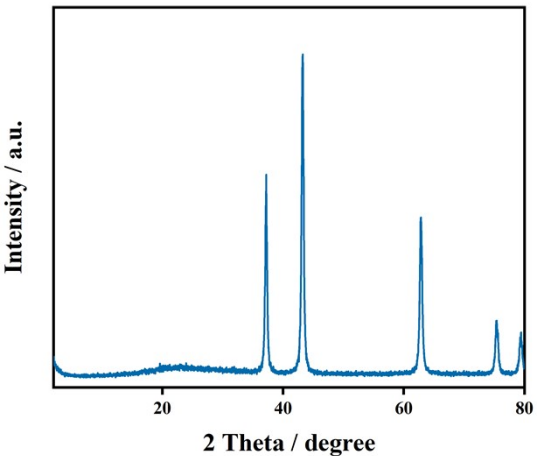

Figure S3. XRD pattern of the product obtained by calcining α-$Ni(OH)_2$ at 800˚C.

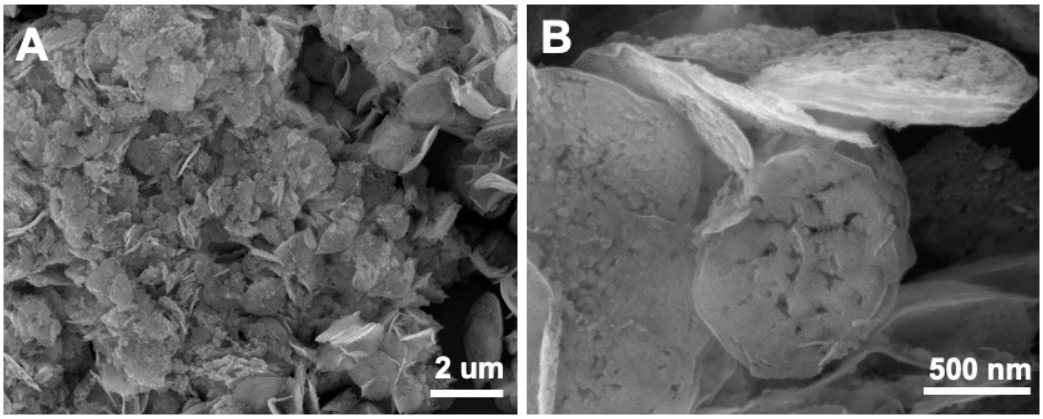

Figure S4. SEM images of porous NiO obtained by calcining α-$Ni(OH)_2$ at 800˚C.

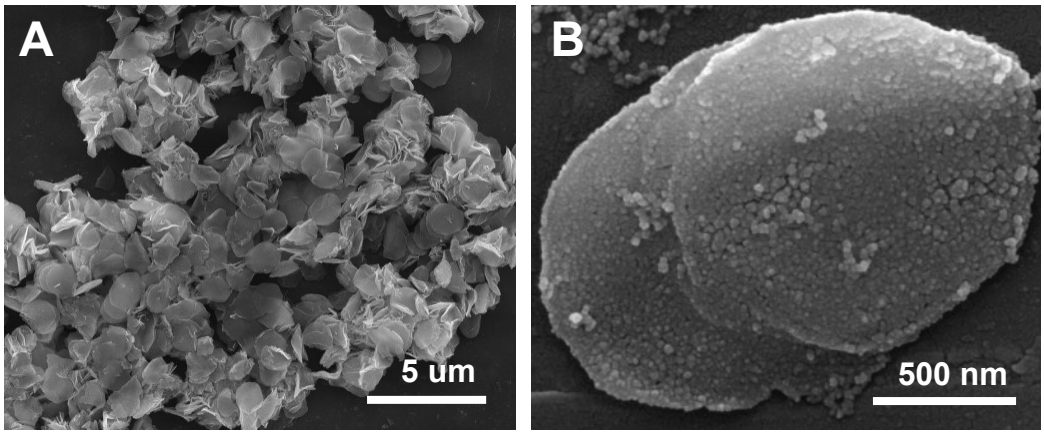

Figure S5. SEM images of porous NiO by calcining α-$Ni(OH)_2$ at 700˚C.

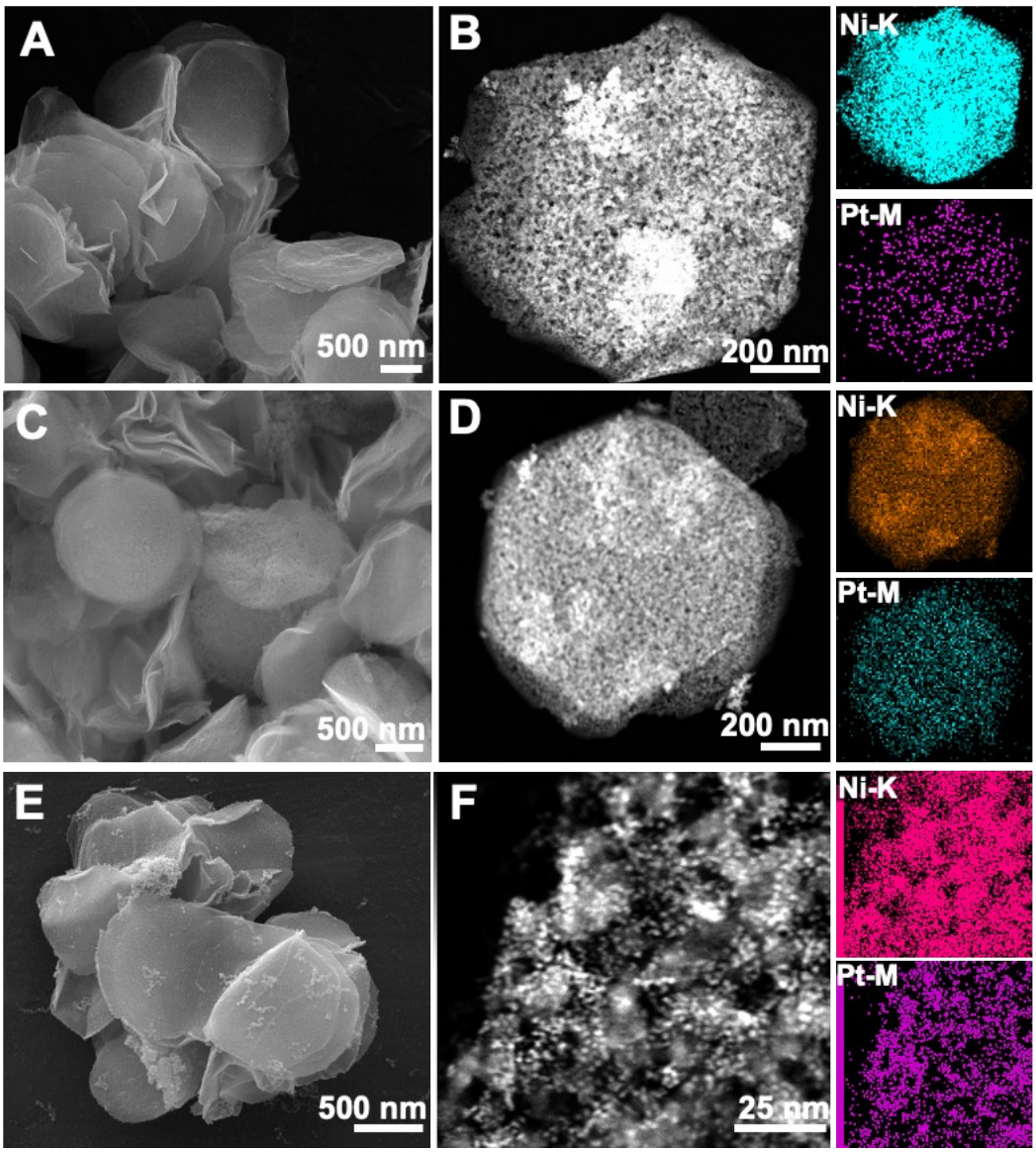

Figure S6. Micro-/nano-structural and compositional characterizations. (A, C, E) SEM images, (B, D, F) HAADF-STEM and corresponding EDX (STEM-EDX) mapping images for (A-B) porous NiO-Pt_{SA}, (C-D) NiO-$Pt_{cluster}$ and (E-F) NiO-$Pt_{particle}$.

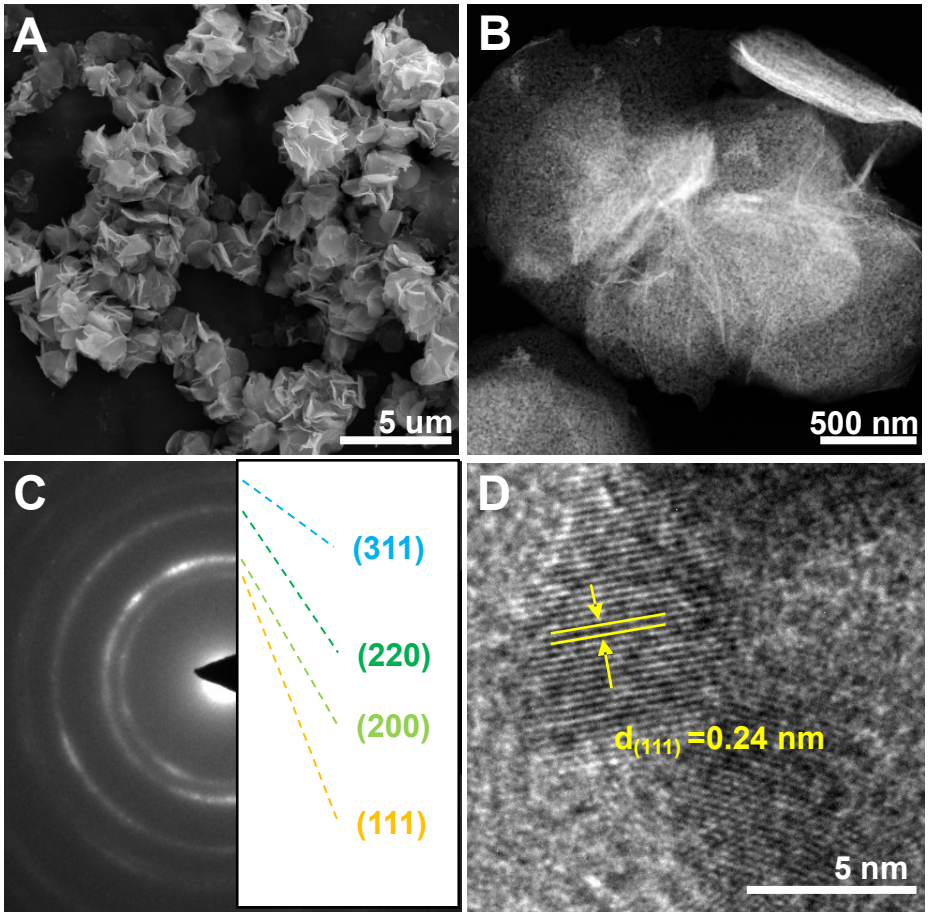

Figure S7. Micro-/nano-structure characterizations of NiO-Pt_{SA}. (A) SEM image, (B) HAADF-STEM image, (C) SAED pattern and (D) HRTEM image.

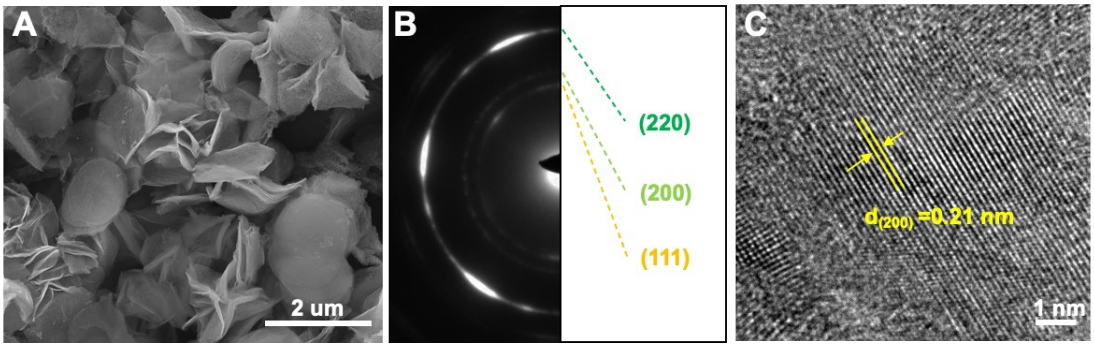

Figure S8. Micro-/nano-structure characterizations of NiO-$Pt_{cluster}$. (A) SEM image, (B) SAED pattern and (C) HRTEM image.

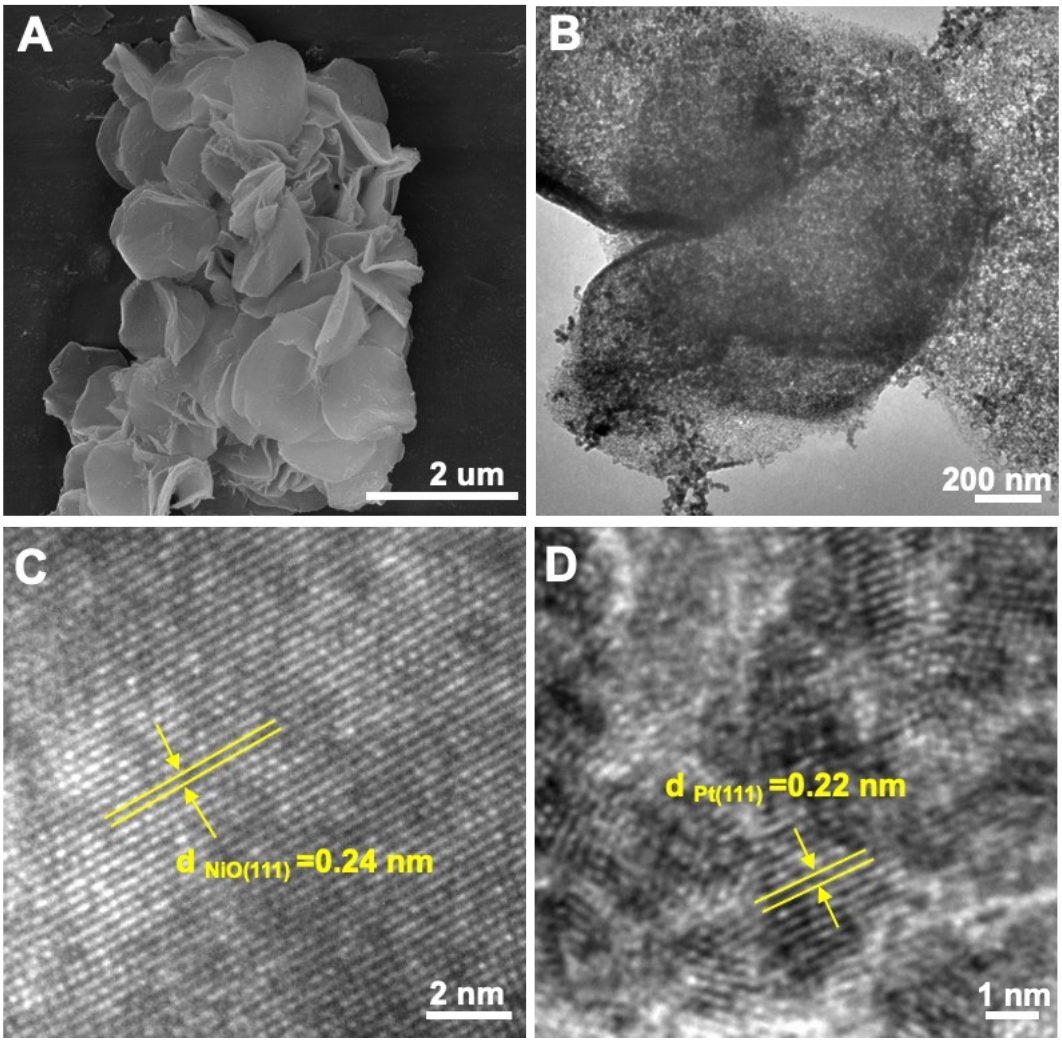

Figure S9. Micro-/nano-structure characterizations of NiO-$Pt_{particle.}$ (A) SEM and (B) TEM images. HRTEM images showing (C) $d_{NiO(111)}$ and (D) $d_{Pt(111).}$

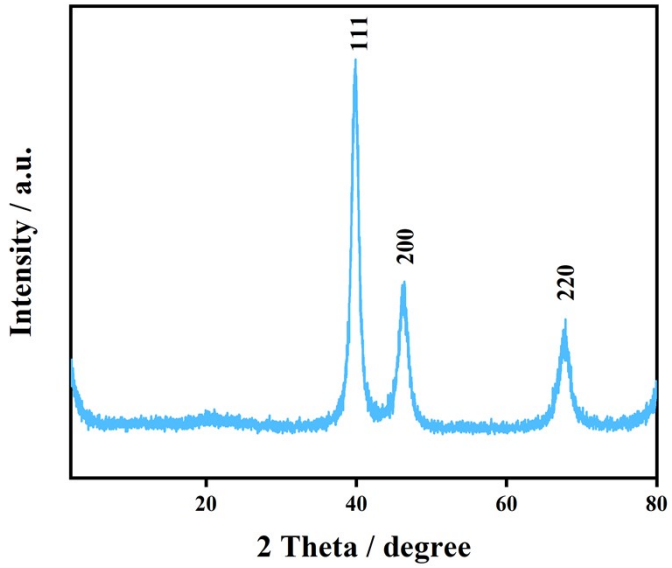

Figure S10. XRD pattern of pure Pt nanoparticles.

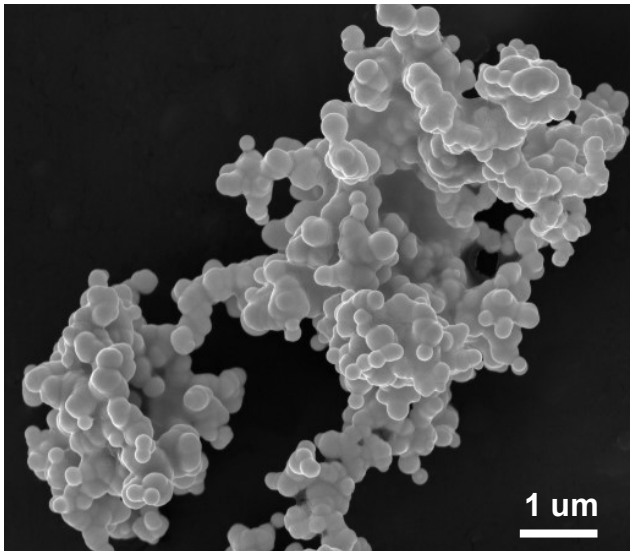

Figure S11. SEM image of Pt nanoparticles.

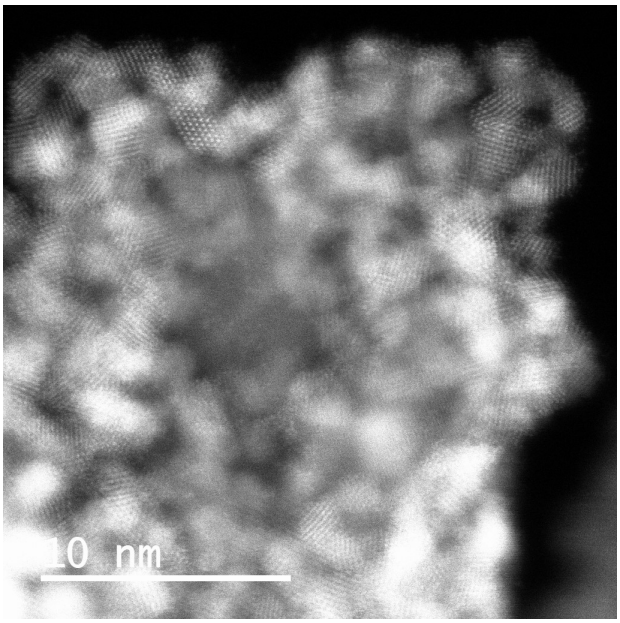

Figure S12. Dark-field HRTEM image of Pt nanoparticles.

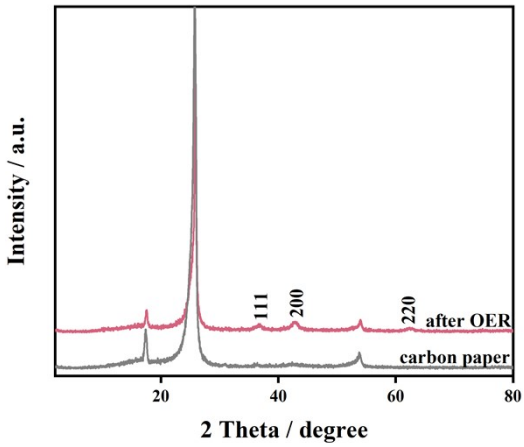

Figure S13. XRD patterns of NiO-Pt_{SA} after OER test and carbon paper substrate.

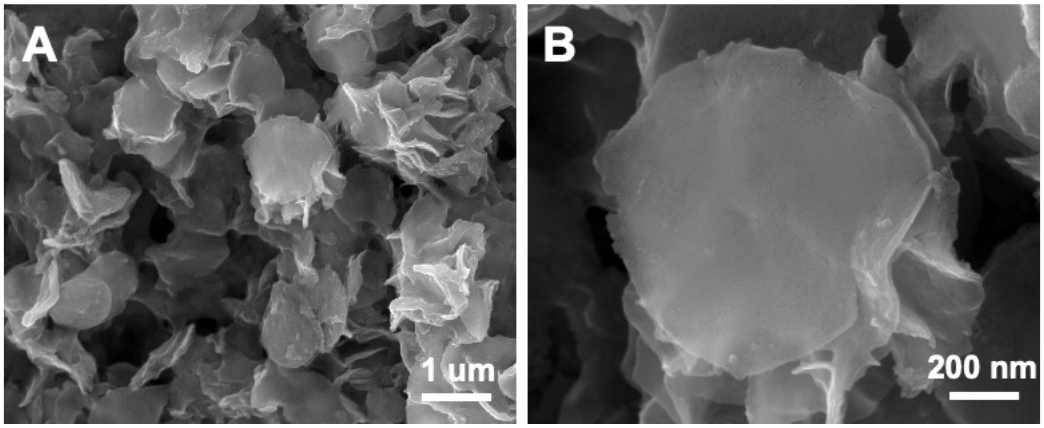

Figure S14. SEM images of NiO-Pt_{SA} after OER test at different magnifications.

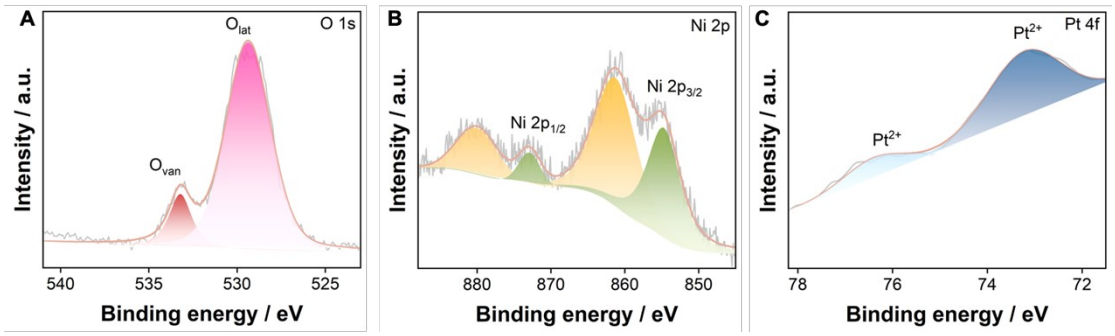

Figure S15. The XPS characterization of NiO-Pt_{SA} catalyst after OER stability. (A) O 1s, (B) Ni 2p, (C) Pt 4f.

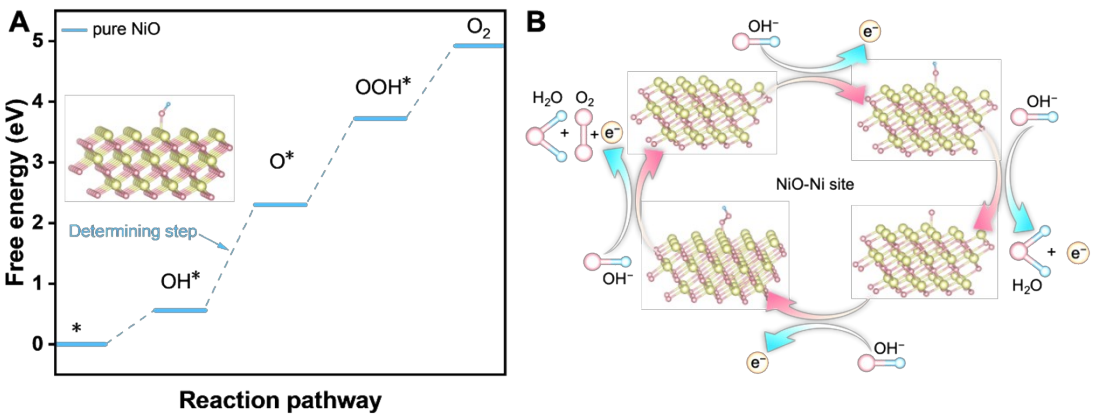

Figure S16. Theoretical calculations toward OER catalyzed by NiO. (A) Free energy diagrams and (B) reaction pathway on Ni sites.

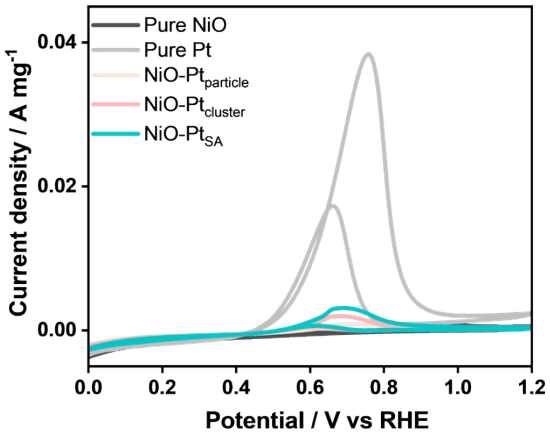

Figure S17. Mass-normalized CV curves of NiO/Pt samples, pure Pt and pure NiO toward MOR.

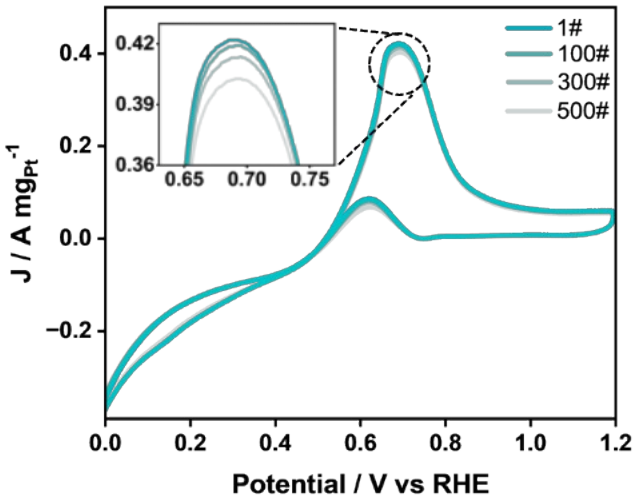

Figure S18. CV curves of NiO-Pt_{SA} after different CV cycles.

Table S1. Fitting R_{ct} values for the as-prepared catalysts toward OER.

catalysts	R_{ct} (Ω)
α-$Ni(OH)_2$	10.6
NiO	8.6
NiO-Pt_{SA}	2.7
NiO-$Pt_{cluster}$	4.4
NiO-$Pt_{particle}$	5.1

Table S2. The atomic content of Pt and Ni in NiO-Pt_{SA} catalyst after OER stability obtained by ICP-OES.

Elements	wt%	at%
Ni	6.24	0.35
Pt	0.037	99.65

Table S3. Fitting R_{ct} values for NiO/Pt catalysts toward MOR.

catalysts	R_{ct} (Ω)
NiO-Pt_{SA}	2478.2
NiO-$Pt_{cluster}$	4312.5
NiO-$Pt_{particle}$	5265.8